Korean J. Chem. Eng., 32(11), 2361-2367 (2015)
DOI: 10.1007/s11814-015-0151-6

pISSN: 0256-1115
eISSN: 1975-7220

Hydrodynamics of multi-sized particles in stable regime of a swirling bed

Chin Swee Miin*, Shaharin Anwar Sulaiman*,†, Vijay Raj Raghavan*, Morgan Raymond Heikal*, and Muhammad Yasin Naz**

*Department of Mechanical Engineering, Universiti Teknologi PETRONAS, 31750 Tronoh, Perak, Malaysia
**Department of Fundamental and Applied Sciences, Universiti Teknologi PETRONAS, 31750 Tronoh, Perak, Malaysia
(*Received 9 February 2015 • accepted 10 July 2015*)

Abstract−Using particle imaging velocimetry (PIV), we observed particle motion within the stable operating regime of a swirling fluidized bed with an annular blade distributor. This paper presents velocity profiles of particle flow in an effort to determine effects from blade angle, particle size and shape and bed weight on characteristics of a swirling fluidized bed. Generally, particle velocity increased with airflow rate and shallow bed height, but decreased with bed weight. A 3° increase in blade angle reduced particle velocity by approximately 18%. In addition, particle shape, size and bed weight affected various characteristics of the swirling regime. Swirling began soon after incipience in the form of a supra-linear curve, which is the characteristic of a swirling regime. The relationship between particle and gas velocities enabled us to predict heat and mass transfer rates between gas and particles.

Keywords: Fluidized Bed, Swirling Regime, Particle Technology, Bed Weight, Blade Angle

INTRODUCTION

Fluidization is an advanced technology with useful and desirable characteristics for a wide variety of industrial applications such as combustion, gasification of biomass fuels, drying, oxidation, metal surface treatment, catalytic and thermal cracking, and coatings [1]. Fluidization technology provides fluid-like behavior for particles by suspending solids in gas [1,2], and has proved useful in numerous chemical and mechanical processes due to its remarkable efficiency and flexibility [3]. Fluidized bed types include the basic conventional approach as well as centrifugal, circulatory, vortex, rotating distribution, rotation with static geometry, toroidal (Torbed), swirling and conical-swirling. In most industrial applications, a conventional fluidized bed utilizes a perforated distributor in which air flows vertically to suspend the particles. However, several drawbacks present challenges, including limited particle momentum (axial only), elutriation, limits on particle size, and large pressure drops.

The swirling fluidized bed (SFB) technique is a new variant in fluidized bed techniques that attempts to overcome the cited conventional fluidized bed disadvantages. SFB minimizes fluid-like momentum axially by transferring it tangentially and radially. Consequently, it reduces pressure drops and provides excellent particle mixing while diminishing elutriation, which allows its application to a wider range of particle sizes.

Fig. 1 shows an SFB design with an annular blade distributor for the inclined injection of gas through the distributor blades. A gas jet entering the bed has two velocity components, vertical and horizontal. The vertical velocity component causes fluidization, while the horizontal component swirls the particles. According to Sreenivasan and Raghavan [2], four regimes operate within the SFB as gas velocity increases. In the first, a 'fixed bed', particles are not fluidized due to the insufficient drag of gas flow that does not overcome particle weight. As gas velocity increases, minimal fluidization occurs as small gas bubbles form at the distributor. This second regime is called 'incipient'. The third regime develops wave-like motions as gas velocity increases and is called a 'slugging bed'. Any further increase in gas velocity weakens this wavy motion, which eventually disappears. As the swirling region widens with further increases in gas velocity, the steady state of swirling particles enter into the fourth regime, which applies to shallow beds. However, if the bed is deep enough, a bi-layered regime forms in which a thin, continuously swirling layer is observed at the bed's bottom with a vigorously bubbling layer at the top.

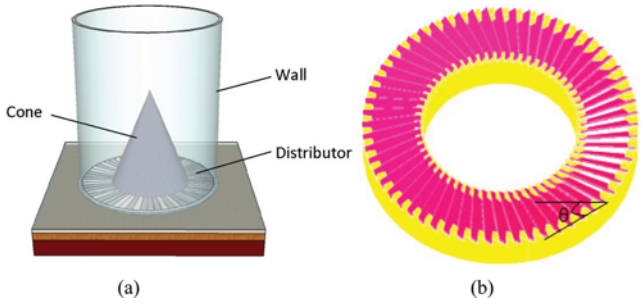

Fig. 1. (a) Annular blade distributor with centre cone; (b) blade angle.

Understanding the velocity profile of particles subjected to SFB treatments is useful in the design and operation of efficient fluidization systems. Nevertheless, experimental studies on SFB particle velocity are sparse. SFBs include the single row vane-type, distributor, blade distributor, inclined hole-type distributor, three row vane-

†To whom correspondence should be addressed.
E-mail: shaharin@petronas.com.my, shaharin@hotmail.com

type distributor, perforated plate distributor, etc. These are used to perform several processes including mixing, coating, classifying, drying, granulation, adsorption, agglomeration, pneumatic transport, and bulk solid heating and cooling. Lee and Liu [3] studied bed expansion and analyzed particle velocity in a cold model, swirling bed combustor that injected a secondary airflow to induce swirling. The secondary air injection did not affect bed expansion but did increase particle velocity. However, particle velocity analysis was based on images taken at the wall and data proved inadequate to analyze particle angular velocity and radial swirling.

Using an annular distributor with a central cone, Vikram et al. developed an analytical model to predict the hydrodynamic behavior of particles in a swirling fluidized bed, to include pressure drop and angular velocity [4]. They reported a linear increase in swirling velocity and quadratic 'bed pressure drop' increases with rising superficial velocity. They concluded that effects from the cone's angle were negligible, while the distributor's blade angle had considerable influence on the bed's characteristics, including bed pressure drop and swirl velocity, both of which decreased with an increase in blade angle. Raghavan et al. adopted this model [5], eliminated the 'lumped model', and then introduced a two-dimensional model (axial and radial) that provided more realistic predictions of SFB hydrodynamic behavior. They reported that superficial velocity and blade angle had more influence on swirl characteristics than other factors, but that large changes in blade angle affect considerable variation in bed characteristics.

Our literature review suggested that SFB annular blade distribution technology has not yet been fully explored [4,5]. A common problem is the inflexibility of blade distributors in the airflow section. Changes in blade width or inclination require complete refabrication of the entire distributor. This fault increases costs and handling complexity in SFB processes, thus, making it difficult to modify existing systems. It also causes unforeseen material wastage, unstable heat transfer, and the corrosion and erosion of fluidized beds, especially when upscaled for commercial use [3]. Such problems are mostly due to a general lack of understanding for characteristic SFB particle dynamics. Hence, the authors determined to examine SFB particle motion and velocity profiles by particle image velocimetry. The current work experimentally establishes effects due to bed weight, blade angle, particle size, and particle shape with a view to provide a more comprehensive understanding of particle motion in the stable swirl regime of a swirling fluidized bed with an annular blade distributor.

MATERIALS AND METHODS

We utilized a laboratory scale SFB to examine effects from particle size and blade angle by particle imaging velocimetry (PIV) on the velocity of particle fields in a fluidized bed.

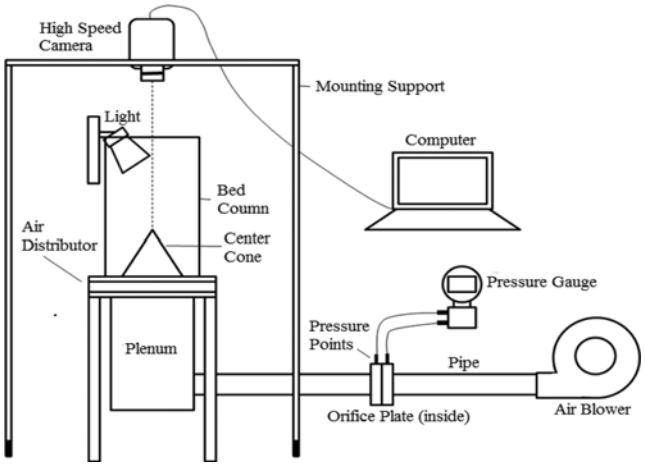

Fig. 2. Schematic of laboratory scale swirling fluidized bed with PIV system.

Table 1. Description of the fluidized bed parameters

Parameter	Description		
Blade angle	12°	15°	18°
Particle size	D=2,900 μm Mass=11.30 mg	D=3,900 μm Mass=23.69 mg	
Particle shape	Spherical D=3,900 μm Mass=23.7 mg	Spheroidal D=3,000 μm H=5,900 μm Mass=24.7 mg	Cylindrical D=1,900 μm L=6,400 μm Mass=35.1 mg
Superficial air velocity	Velocity ranges in steady state swirling regime of operation and early bubling regime of operation		
Bed weight (g)	500, 750, 1000, 1250, 1500		

1. Experimental Setup

Fig. 2 shows the complete experimental setup comprising a laboratory scale swirling fluidized bed with an annular blade distributor. Sixty blades were arranged on outer and inner aluminum holders with a hollow metal cone (20 cm in diameter), placed in the center of the bed along with a 30 cm diameter acrylic glass (Plexiglas) bed column fixed to the bed. The bed column was 60 cm in height. A plenum chamber height of 50 cm ensured smooth airflow and steady up-flow into the fluidized bed through the distributor.

A 5.5 kW high-pressure blower injected air with a maximum static pressure of 600 mm wg (rated flow at 1,000 m^3/hr) through a 10 cm diameter pipe connected to the wind box at the bottom of the fluidized bed. A motorized controller governed the air blower's airflow rate. The pressure differential, as measured across the orifice plate, located in the pipeline (Fig. 2), was used to calculate the superficial velocity of air entering the distributor. A Phantom v9 high-speed camera custom mounted to allow imaging from the top of the bed (160 cm above the fluidized bed) enabled PIV measurements.

Table 1 illustrates parameter descriptions for this experiment. Blades with 12, 15 and 18° angles were fabricated for comparative evaluations. Except for effects deriving from the blade's angle, the 15° angle blade was used for all trials. Due to uniformity in size and shape, spherical PVC particles resulting in beds of mono-sized particles (3,900 and 2,900 μm diameter, respectively), were used to investigate effects deriving from particle size. Effects from particles of different densities were not studied. Spherical, spheroidal (rice-shaped) and cylindrical particles were chosen for particle shape comparisons as they commonly represent particles in applications and are used as catalysts, medicine pills, biomass briquettes, etc. All other experiments utilized spherical particles. Table 2 shows adjustments in superficial air velocity entering the bed within range of stable swirl regimes for operations using bed weights from 500 to 1,500 g at increments of 250 g.

Table 2. Velocity profiles of 2,900 μm spherical particles in a 750 g swirling bed with increasing superficial velocity of air

Superficial air velocity (m/s)	Velocity profile	Average particle velocity (m/s)
1.60		0.72
1.75		0.80
1.90		0.83
2.02		0.84
2.14	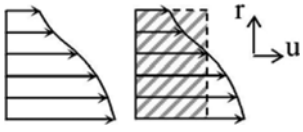	0.92

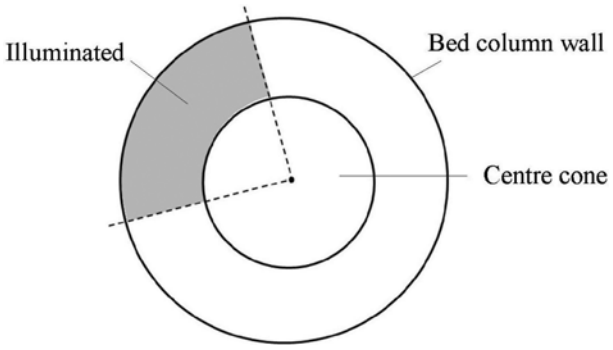

Fig. 3. Illuminated bed section viewed from the top.

2. Particle Imaging Velocimetry

Initial PIV settings found that particles flowing in the fluidized bed were too dense; hence, image analysis was not possible. To distinguish particle motion, white particles were used as tracers, along with black or blue particles, because their light reflection better enabled the assay. Laser sheeting and background fluorescent illumination were not applied as the system was opaque and observation was limited to the bed's top layer. Hence, only a quarter of the bed (Fig. 3) was photographed at any given moment since, as reasonably assumed, the circular motion of all particles was uniform. A 50-W halogen lamp was used to illuminate the bed's upper layer.

Images of particle flow were recorded by high-speed camera at a resolution of 864×856 pixels. Frame rates varied from 1,200 to 2,000 pictures per second (pps) to match illumination conditions and particle velocity. The binary image cross-correlation method (BICC) was used to measure displacement velocity. Our method of analysis employed an algorithm for particle distribution pattern tracking in which the motion of each tracer particle was tracked based on the highest similarity of particle distribution patterns between two-consecutive images [6]. To execute image processing, MATLAB software was employed along with a program applying the BICC method. Initial velocity fields were filtered with a signal-to-noise ratio filter, as well as global and local filters. Eliminated noise and vectors left gaps in the velocity field that were filled by interpolating neighboring velocities to obtain a complete velocity field. These procedures were repeated for 28 trial sets by changing parameters as shown in Table 1.

RESULTS AND DISCUSSION

Four different regimes, namely, packed bed, slug-wavy, swirling and bi-layer, are commonly observed in SFB. However, none are thus far fully understood [6,7]. Therefore, to better understand the bed's behavior under different modalities, it is important to identify and classify these regimes. An optimized regime for any process can only be determined once all regimes have been properly

investigated. Kumar et al. [7] revealed the sequence of SFB flow regimes in SFB as packed bed, minimum fluidization, swirling regime, two-layer regime and finally, elutriation or transport. As superficial velocity increases, the state of the bed changes from a packed bed to minimum fluidization followed by the slug-wavy and swirling regimes. In the swirling regime, particles in the bed begin their suspension and swirl in the air column closest to the distributor. This regime is the focus of the current study as it holds significant industrial importance. Beyond this, any further increase in superficial velocity may result in elutriation, which is normally avoided during a fluidized bed operation.

The PIV program generated velocity vector fields of particles suspended at the top of the bed. Fig. 4 illustrates a typical velocity vector field obtained for a 750 g bed of 2,900 μm spherical particles at a superficial air velocity of 2 m/s. The velocity field shows particle trajectory and velocity magnitude in m/s. Velocity profiles for every 15° angle referenced to the bed's center derive from the velocity vector field. Fig. 5(a) shows a typical plot of a velocity vector profile as the result of local averaging. Fig. 5(b) shows a typical individual velocity profile indicating average (shaded area) and maximum particle velocities along a line between the wall and the cone.

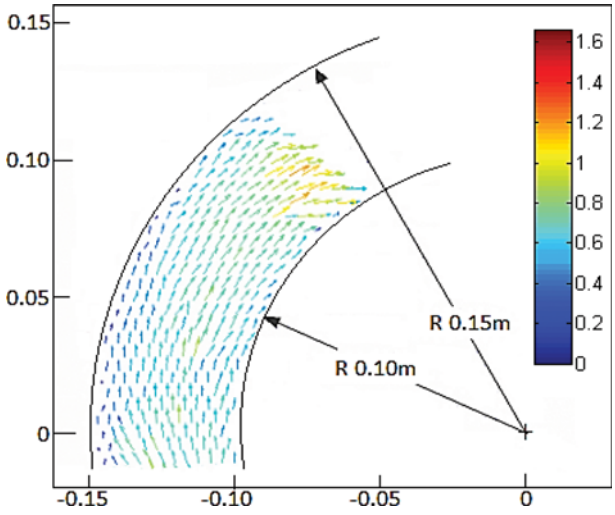

Fig. 4. A typical velocity vector field of the swirling bed.

Fig. 5(a) demonstrates that highest particle velocities occurred near the cone or midway between the cone and the bed column wall. However, different velocity profile patterns were obtained depending on superficial air velocity [7,8]. Table 2 shows a velocity profile for 2,900 μm spherical particles within a 750 g swirling bed with increasing superficial air velocity. At a lower superficial velocity, particle motions near the bed wall and center cone were slowed by friction. Particles in contact with the center cone's surface had the lowest velocity, while particles in the middle region had the highest velocity [9,10]. As superficial velocity increased, velocity near the surfaces also increased because swirling momentum was sufficient to overcome friction, mainly because tangential centrifugal forces caused the particles to move further from the cone, thus reducing friction and increasing particle swirl velocity. Particle velocity near the center cone increased with superficial air velocity, while particle velocity closest to the column wall remained low, regardless of any increase in superficial air velocity. This was due to the centrifugal force that increased with superficial air velocity; hence, resulting tangential particle motions on the column wall kept their momentum closer to the wall, consequently increasing inter-particle and surface friction.

1. Effect of Bed Weight

Fig. 6 shows variation in particle velocity as a function of superficial air velocity for 3,900 μm spherical particles at bed weights between 500 and 1,500 g. In general, particle velocity decreased with increased bed weight due to an associated increase in the bed's height. The observed particle velocity, as recorded, pertains to the uppermost bed layer. As the air jet percolated through the bed, its velocity continually decreased due to a transfer of momentum to the particles. Consequently, particle velocity in the uppermost layer decayed as the bed's height increased.

As made evident by the steepest gradient shown in Fig. 6, parti-

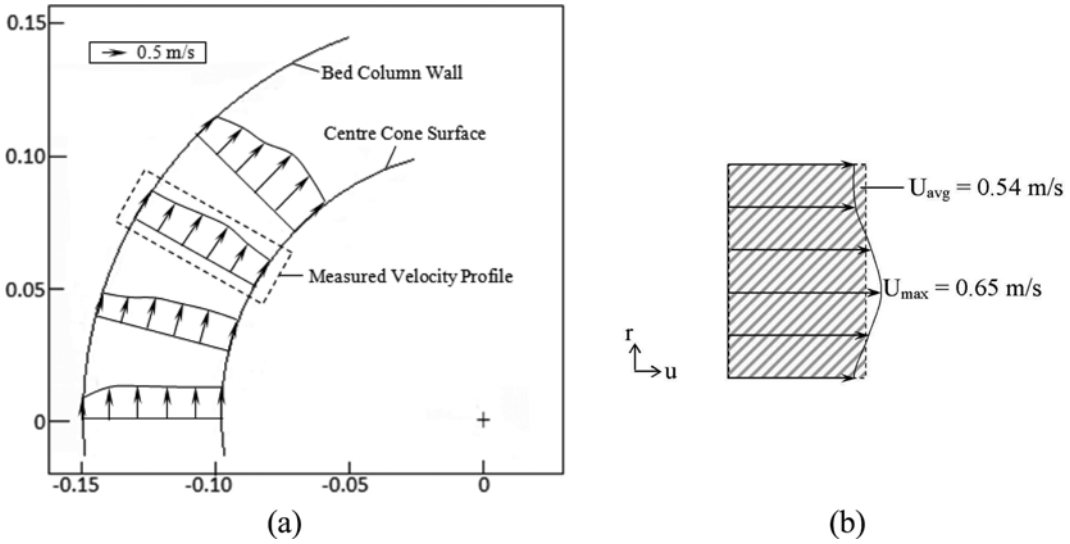

Fig. 5. Particle velocity vector profiles: (a) camera's field of view; (b) typical individual velocity profile.

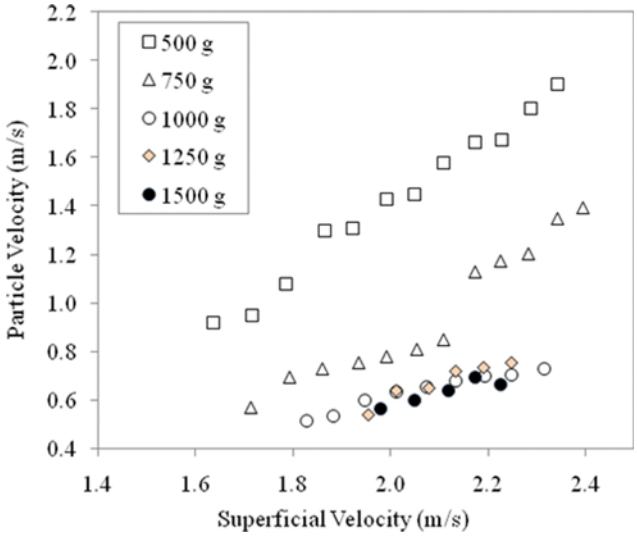

Fig. 6. Variation of particle velocity for different bed weights of 3,900 μm spherical particles.

cle velocities for the 500 g bed were the most sensitive to changes in superficial air velocity. An increase in bed weight caused particle velocity to be less sensitive to changes in superficial velocity. Furthermore, Fig. 6 clearly indicates that the minimum swirling superficial air velocity increased with bed weight. The upper limit of the swirling superficial air velocity also decreased with bed weight. These trends likely derived from heavier beds as greater numbers of particles caused increased friction between particles and the wall, thus requiring a higher air momentum to swirl the particles [11,12].

Fig. 6 also shows that particle velocity for bed weights >1,000 g remained almost constant, regardless of any increase in bed weight because particles were actually moved by the expansion of bubbles, which were neither vigorous nor random. Instead, their occurrence was consistent and less dynamic, providing a constant trend in velocity. Interestingly, the 750 g bed displayed a similar trend of near-constant particle velocity. However, this trend changed after the superficial velocity of air reached 2.2 m/s, suggesting that similar turning points exist for bed weights between 500 and 1,000 g.

2. Effect of Blade Angle

Fig. 7 shows typical variation in particle velocity for superficial air velocity at blade angles of 12, 15 and 18° for 3,900 μm spherical particles (500 g bed weight). This bed weight was chosen because of its sensitivity to superficial air velocity. Fig. 7 shows that stable swirling occurred only at superficial air velocity >1.8 m/s, below which, bubbling and slugging regimes occurred. As expected, particle velocity increased with superficial air velocity. However, particle velocity decreased with increases in blade angle. A plausible explanation is that a larger blade angle results in higher surface friction due to a larger surface area for particle contact. Furthermore, blades with a wider angle have greater mass compared to those with narrower angles, thus increasing air flow disturbance with consequent increases in pressure drops. From this analysis, the authors concluded that a 3° increase in blade angle caused a particle velocity reduction of approximately 18%.

Raghavan et al. [5] observed that superficial velocity and blade angle have greater influences on swirl characteristics than those of other parameters. However, large changes in blade angle can cause considerable variation in bed characteristics. When gas penetrates more deeply into the bed, horizontal angular momentum is transferred to the particles. As a consequence, the horizontal component of gas velocity decays and gas flow turns vertically. In deep beds, a point is reached where the gas flow becomes almost completely vertical, which results in multi-layer fluidization with a shallow, continuously swirling lower layer and vigorously bubbling upper layer [13-16]. Sreenivasan and Raghavan [2] posited that considerable radial variation in particle angular velocity was undesirable due to larger energy and momentum losses caused by inter-particle shearing. As such, this indicates the need to redesign the distributor to produce a more uniform gas flow. Despite the good qualities of a swirling fluidized bed, at very high superficial velocity, bed

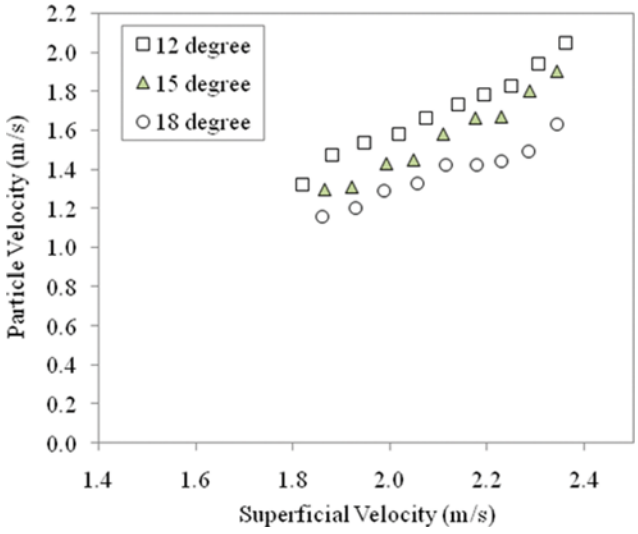

Fig. 7. Variation of particle velocity for different blade angles.

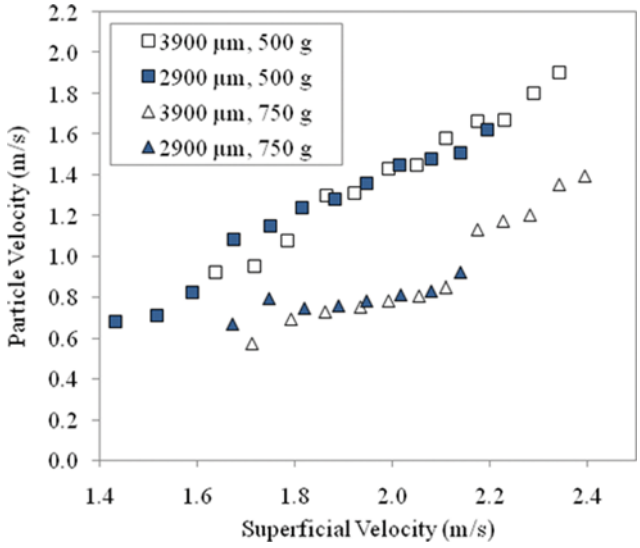

Fig. 8. Variation of particle velocity for different spherical particle sizes.

particles begin to fly towards the periphery only to create an annular dead zone with gas bypass at the center. Consequently, the available annular area is only partially utilized at higher velocities.

3. Effect of Particle Size

Fig. 8 shows velocity variations for 3,900 and 2,900 μm spherical particles with superficial air velocity and bed weights of 500 and 750 g. Only two bed weights were available for comparison, mainly because 2,900 μm spherical particles have no stable operative swirling regime when their bed weight exceeds 750 g.

Overall, particle velocities for both particle sizes increased with superficial air velocity. However, smaller spherical particles had a lower minimum swirling superficial air velocity. The 500 g bed weight of smaller spherical particles began to swirl at a superficial air velocity of approximately 1.4 m/s. Larger spherical particles achieved stable swirling at 1.6 m/s. Fig. 8 shows that the maximum superficial air velocity for a stable swirling regime was lower for smaller particles (about 2.2 m/s), compared to larger particles (~2.4 m/s). A similar trend was observed in the 750 g bed, although smaller particles had a narrower band where superficial velocity sustained a stable swirling regime. Thus, the authors propose that a smaller particle size is preferred for applications with shallow beds because lower superficial air velocity is sufficient to initiate and sustain swirling, which implies less energy consumption [13-15].

Generally, we noted that graphs of particles of the same bed weight coincided, although distinct differences occurred when approaching minimum and maximum particle velocities. This suggested that, apart from minimum and maximum particle velocities, inter-particle spaces for different particle sizes probably have insignificant effects on particle velocity compared to effects from bed weight [13-16].

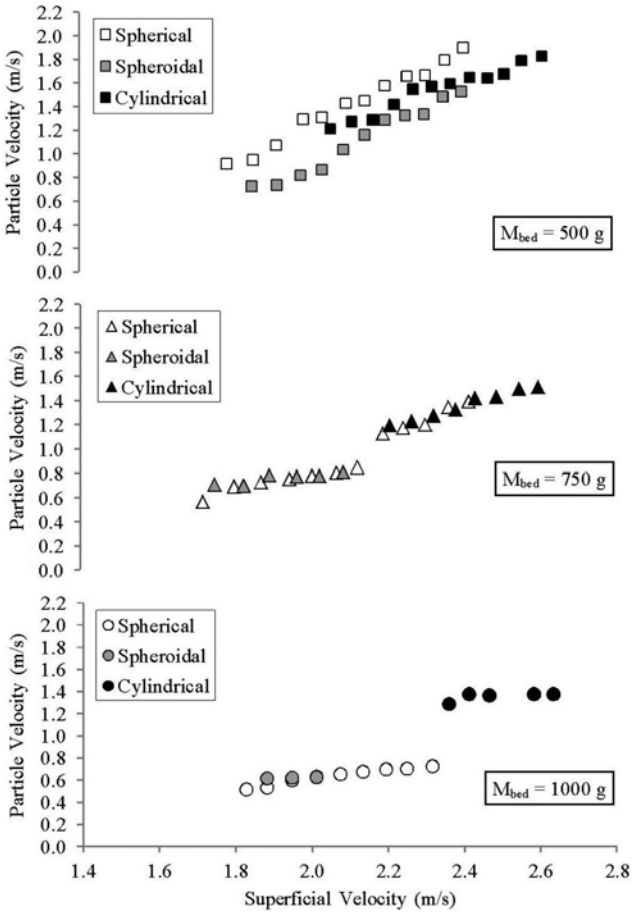

Fig. 9. Variation of particle velocity for different particle shapes.

4. Effect of Particle Shape

Fig. 9 shows variations in particle velocity for spherical, spheroidal and cylindrical particles at different superficial air velocities and bed weights ranging from 500 to 1,000 g. Table 1 presents individual mass and particle size for each shape. Particle velocities increased with superficial air velocity regardless of shape. Nevertheless, when bed weight was increased for all shapes, variation in particle velocity decreased, likely due to the constant bubbling described earlier as a direct effect of bed weight. Similar to the trend shown in Fig. 8, regardless of shape, graphs of our results for particles of the same bed weight coincided, as shown in Fig. 9. Differences were observed only for minimum and maximum particle velocities in the stable swirling regime, which implies minimal effects from inter-particle properties on particle velocity [17,18].

Fig. 9 shows that both spherical and spheroidal particles began swirling at approximately the same superficial air velocity, yet the observed spheroidal particle velocity was slightly lower. This reduction was likely due to increased interfacial friction as a result of larger particle surface area. However, this did not apply to heavier bed weights of 750 and 1,000 g as particle velocity graphs for both shapes at these weights overlap (Fig. 9). This suggests that bed weight overcomes some effects from particle shape as the bed becomes heavier. Spheroidal particles of 750 and 1,000 g bed weights also had markedly reduced, stable swirling ranges due to a vigorous bubbling layer, likely because spheroidal particles elevate more readily due to their larger surface areas, which results in higher lift forces [5, 19,20].

Compared to spherical particles, the spheroidal particles were more compacted as they have less sphericity and greater overall bed density due to reduced interstitial spaces. The absence of voided space when compacted should carry through to the fluidized state. However, sphericity appears to have a distinct effect here because uniform spheres pack more compactly. Their slugging period is longer, although the slugging velocity range is the same. As sphericity decreases, particles appear to undergo slugging more readily. The small fluidization velocity of spheroidal particles appears to generate the highest bed expansion [4,5,21].

We noted that the narrow swirling range did not occur with cylindrical particles with their larger surface area. The explanation is that cylindrical particles are heavier, which reduces bubbling. The cylindrical particles shown in Fig. 9 had a higher minimum superficial air velocity, which upwardly shifted the stable swirling range because their heavier mass increased inertia, which, in turn, required higher air momentum for mobilization [18,19].

With increased bed weight, the velocity gap between cylindrical and other particle shapes widened. This indicated that cylindrical particle velocity did not decline as much as spherical and spheroidal particle velocities as bed weight increased. Spherical and spheroidal particle velocities declined more due to the deeper bed height that attenuated the transfer of air-jet momentum to the upper layer

particles. On the other hand, cylindrical particles produced shallower beds because fewer particles were needed to achieve the same bed weight by comparison. Hence, air-jet momentum was more efficiently transferred to upper layer particles.

Our results suggest that spherical particles better suit industrial applications due to their ability to sustain a more stable swirling flow under a broader range of superficial airflow velocity. In addition, they require a relatively lower minimum swirling superficial air velocity, which directly implies a more efficient and higher transfer of momentum, indicating lower energy requirements for processing applications. Spheroidal particles experienced a narrow stable swirling range due to bubbling that can likely be remedied by using heavier particles such as the cylindrical particle. Even so, a larger swirling superficial air velocity would be required.

CONCLUSIONS

The swirling fluidized bed has four operant regimes: incipient, partial swirling, stable swirling, and bi-layered fluidization for deeper beds. This paper specifically addressed effects from blade angle, particle size, particle shape, and bed weight on particle motion during the stable swirling regime. The analysis allows the following conclusions:

- Decreased particle velocity with increased bed weight and decreased superficial airflow velocity correlates well with theory.
- Particle velocity decreased by nearly 50% when bed weight increased by 50% for a light bed of 500 g. However, greater increases in bed weight (>1,000 g) did not cause any significant decrease in particle velocity, mainly because particles moved as a result of bubble expansion.
- Decreasing superficial velocity generally causes a linear decrease in particle velocity, although a lightweight bed was more sensitive to the change compared to heavier beds. An increase in bed weight caused particle velocity to become less sensitive to changes in superficial velocity. Heavier beds had larger numbers of particles resulting in higher inter-particle friction as well as greater friction between particles and the wall, thus, requiring higher air momentum to swirl the particles.
- An increase in the blade angle caused a significant reduction in particle velocity due to an associated increase in friction and pressure drops. The authors determined that a 3° increase in blade angle caused an approximate 18% reduction in particle velocity.
- Smaller spherical particles had a lower minimum swirling superficial air velocity than larger spherical particles (up to 11%). Moreover, the maximum superficial air velocity for a stable swirling regime was lower for smaller particles (~2.2 m/s) compared to larger particles (~2.4 m/s). Hence, we posit that smaller particles swirl more easily when constrained by a shallow bed.
- Spherical particles demonstrated a broader stable swirling range and required lower swirling superficial air velocity. Spheroidal particles showed a narrower stable swirling range due to bubbling. Heavier cylindrical particles reduced bubbling motion at the cost of raising higher superficial air velocity. As superficial velocity increased, the state of the bed changed from packed to minimal fluidization, then to slug-wavy followed by swirling and a vigorously bubbling bed with lower layer swirling. Hence, when beds are deep, a bi-layer regime can also occur. To understand bed behavior under different modalities, it is important to identify and classify these regimes.

ACKNOWLEDGEMENT

The Science Fund, No. 03-02-02-SF0091, under the Ministry of Science, Technology and Innovation Malaysia, funded this project. The authors express their heartfelt gratitude to Drs. Yohannes T. Anbese and Vinod K. Venkiteswaran for their valuable assistance.

REFERENCES

1. H. Cho, G. Han and G. Ahn, *Korean J. Chem. Eng.*, **19**, 183 (2002).
2. B. Sreenivasan and V. R. Raghavan, *Chem. Eng. Process*, **41**, 99 (2002).
3. S. W. Lee and Y. Liu, *Can. J. Chem. Eng.*, **82**, 1054 (2004).
4. G. Vikram, H. Martin and V. R. Raghavan, *The swirling fluidized bed - an advanced hydrodynamics analysis*, 4th National Workshop & Conference on CFD Technology & Revamping of Boilers, Shibpur, India (2003).
5. V. R. Raghavan, M. Kind and M. Martin, *Modelling of the hydrodynamics of swirling fluidized beds*, 4th European Thermal Sciences Conference (EUROTHERM) & Heat Exchange Engineering Exhibition, Birmingham, UK (2004).
6. H. Abdulmouti and T. M. Mansour, *The technique of PIV and its applications*, 10th International Congress on Liquid Atomization and Spray Systems, Kyoto, Japan (2006).
7. V. V. Kumar, M. Faizal and V. R. Raghavan, *Eng. e-Trans.*, **6**, 70 (2011).
8. R. Kaewklum and V. I. Kuprianov, *Chem. Eng. Sci.*, **63**, 1471 (2008).
9. N. Ellias, H. T. Bi, C. J. Lim and J. R. Grace, *Powder Technol.*, **98**, 124 (2004).
10. D. Cho, J. H. Choi, M. S. Khurram, S. H. Jo, H. J. Ryu, Y. C. Park and C. K. Yi, *Korean J. Chem. Eng.*, **32**, 284 (2015).
11. J. M. Valverde, F. Pontiga, C. Soria-Hoyo, M. A. S. Quintanilla, H. Moreno, F. J. Duran and M. J. Espin, *Phys. Chem. Chem. Phys.*, **13**, 4906 (2011).
12. K. J. Whitty and M. Siddoway, *Rev. Sci. Instrum.*, **81**, 73305 (2010).
13. B. Chalermsinsuwan, T. Thummakul, D. Gidaspow and P. Piumsomboon, *Korean J. Chem. Eng.*, **31**, 350 (2014).
14. P. D. Hede, P. Bach and A. D. Jensen, *Ind. Eng. Chem. Res.*, **48**, 1914 (2009).
15. R. S. Saksena and L. V. Woodcock, *Phys. Chem. Chem. Phys.*, **6**, 5195 (2004).
16. P. D. Hede, P. Bach and A. D. Jensen, *Ind. Eng. Chem. Res.*, **48**, 1905 (2009).
17. J. H. Choi, C. K. Yi and J. E. Son, *Korean J. Chem. Eng.*, **7**, 306 (1990).
18. D. Sathiyamoorthy and H. Masayuki, *Chem. Eng. J.*, **93**, 151 (2003).
19. C. Wang, Z. Zhong and X. Wang, *Korean J. Chem. Eng.* (2015), DOI:10.1007/s11814-015-0033-y.
20. J. M. Valverde, F. Pontiga, C. Soria-Hoyo, M. A. S. Quintanilla, H. Moreno, F. J. Duran and M. J. Espin, *Phys. Chem. Chem. Phys.*, **13**, 14906 (2011).
21. J. Kim, G. Han and C. Yi, *Korean J. Chem. Eng.*, **19**, 491 (2002).